Article

Screening of the Au:Pt Atomic Ratio Supported in SrCO₃: Effects in the Performance of the Solvent-Free Oxidation of Benzyl Alcohol

Francisco S. C. L. Batista,[a] Itaciara E. M. S. Melo,[a] Laíse N. S. Pereira,[a] Alexia G. P. Lima,[a]
Ali H. Bashal,[b] Jean C. S. Costa,[a] Janildo L. Magalhães,[a] Francisco C. A. Lima,[c,d]
Carla V. R. Moura, [*,a] Marco A. S. Garcia* [a] *and Edmilson M. Moura* [a]

[a]Departamento de Química, Universidade Federal do Piauí, 64049-550 Teresina-PI, Brazil

[b]Department of Chemistry, Faculty of Science, Taibah University,
30002 Al-Madinah Al-Mounawara, Saudi Arabia

[c]Programa de Pós-Graduação em Biotecnologia (RENORBIO),
Universidade Federal do Piauí, 64049-550 Teresina-PI, Brazil

[d]Laboratório de Quântica Computacional e Planejamento de Fármacos,
Universidade Estadual do Piauí, 64002-150 Teresina-PI, Brazil

We have prepared, by a sol-immobilization method, bimetallic catalysts with different Au:Pt atomic ratios supported on commercial SrCO₃. The catalytic performance for the oxidation reaction of benzyl alcohol of such materials was compared to the monometallic counterparts, aiming at the obtaining of the best composition of the material. It was found that the Au:Pt atomic ratio presents a remarkable effect on the system performance, i.e., Pt-rich systems are more selective; however, less active. Thus, an equilibrium related to the activity and selectivity of the system was obtained by considering the yield of the system. Also, some density functional theory (DFT) insights were obtained by using a cluster of 14 atoms of Au and 1 or 2 atoms of Pt. X-ray photoelectron spectroscopy, elemental mapping in scanning transmission electron microscopy before and after catalyst usage, flame atomic absorption spectroscopy, Rietveld refinement, among other techniques, were used and associated to the experimental data, which allowed us to propose a catalytic mechanism for the system, which was important since SrCO₃ has not been considered before as catalyst support for alcohol oxidation reactions.

Keywords: oxidation, AuPt nanoparticles, SrCO₃, mechanism

Introduction

Optimizing bimetallic systems by exploring their electronic and structural effects is essential for the design of new and more efficient catalysts.[1-3] Although Pt and Pd nanoparticles (NPs) were the first catalysts to present activity in oxidation reactions,[4,5] their deactivation is a great issue, which is difficult to solve due to their easy overoxidation and poisoning from byproducts.[6] When Au NPs were found to be very active and selective for oxidation reactions by Prati and co-workers,[7-9] and more robust with respect to deactivation processes, their utilization dramatically increased. However, mixing Au NPs with Pt or Pd NPs have demonstrated the possibility of merging

reproducible synthesis with structure-activity relationships, which presents advantages in terms of catalyst performance and stability.[10-13]

The exceptional performance of bimetallic catalysts when compared to monometallic ones is not fully understood due to the possibility of different combinations among reactants, composition, and reaction conditions,[14] which usually provides only isolated applications. However, massive experimental data showed that alloying Au with Pt promotes a remarkable synergy in the oxidation of alcohols, which involves electronic changes that act on the strength of adsorbed species, suppressing poisoning;[15] a feature highly desired for catalytic applications. Thus, several examples are demonstrated in the literature. An example was published by Tan *et al.*[16] They have reported that non-supported AuPt NPs exhibited improved electrochemical

*e-mail: carla@ufpi.edu.br

performances when compared to the commercial Pt/C catalysts by preventing agglomeration, which impacted in the long-term stability of the material for the oxidation of methanol.

Due to economic issues, catalyst supports are aimed in heterogeneous catalysis. Nevertheless, beyond the separation requisite, the support choice is crucial for the rationalization of a novel material since it can strongly influence the performance of a catalyst regarding its activity and selectivity due to metal-support interactions.[17] In the literature, AuPt bimetallic systems are observed to be immobilized on different supports, for several applications. Brett *et al.*[18] have demonstrated that AuPt NPs supported on MgO and hydrotalcite produced glyceric acid from glycerol in a selectivity range of 73-78%. Also, Corma *et al.*[19] have already long stated that earth metal oxides and hydroxides are important for base-catalyzed reactions, although they do not seem much explored in the literature. Our group has been working on the successful utilization of strontium-based supports for the oxidation reaction of benzyl alcohol. We have been exploring the use of $Sr(OH)_2$,[20,21] which presented remarkable stability as catalyst support. Also, the material allowed the application of the catalyst without external base addition with noteworthy results. However, $SrCO_3$ was not studied by us and, as far as we can tell, by others. The importance of its use is its direct application on the catalyst synthesis as the $Sr(OH)_2$ obtaining requires a calcination step at very high temperatures (usually, close to 1100 °C or higher). In addition, just a few studies have been working on the AuPt atomic/molar ratio for selective oxidation of alcohols.[22-24] Herein, we used benzyl alcohol oxidation as a model reaction since we are studying a new catalytic system. However, the selective oxidation of alcohols is highly important once the selectivity to the partially oxidized product is more difficult to obtain; thus, benzaldehyde is the desired product in our studies.

For the first time, commercial $SrCO_3$ was selected as the support for bimetallic systems with different Au:Pt atomic ratios; the insertion of Pt atoms was studied for the selectivity improvement of the system, which showed to be highly efficient. We intended to present a stable and easy-to-synthesize material, which presented recyclability. The catalysts were used in the solvent-free oxidation of benzyl alcohol in the presence of K_2CO_3, and the best atomic ratio composition was selected. We started our studies by considering density functional theory (DFT) calculation insights that showed that highest occupied orbital-lowest unoccupied orbital (HOMO-LUMO) gap energies were favored by the addition of a second Pt atom on an Au cluster, which was experimentally proved beneficial for the performance of the catalyst. Thus, bearing in mind

the yield of the system, we characterized a chosen system by X-ray photoelectron spectroscopy (XPS), elemental mapping in scanning transmission electron microscopy (STEM) before and after catalyst usage, flame atomic absorption spectroscopy (FAAS), and X-ray diffraction (XRD), among other techniques, which gave us subsidies, associated with the experimental data, to propose a catalyst mechanism for the system.

Experimental

Materials

All the materials used herein were of analytical grade (bought from Sigma-Aldrich, São Paulo, Brazil) and used as received, without further purification.

Catalyst preparation

The catalysts were synthesized by using a sol-immobilization method described elsewhere, with some modifications.[25] Considering that some different Au:Pt atomic ratios were used, the preparation of the $Au_{14}Pt_2/SrCO_3$ catalyst is explained here; however, using the same procedure and varying the Au:Pt ratio, the following catalysts were prepared: $Au_{14}Pt_{10}$, $Au_{14}Pt_{14}$, $Au_{14}Pt_{28}$, and $Au_{14}Pt_{42}$, individually supported in $SrCO_3$. All the catalysts were produced to present 2.0 wt.% of metal on the support. In a typical procedure, 25 mL of an aqueous solution with 52.27 mg of gold(III) chloride ($HAuCl_4$, 30 wt.% diluted in HCl, 99.99% trace metals) were mixed with 25 mL of an aqueous solution with 1.84 mg of sodium tetrachloroplatinate(II) hydrate ($Na_2PtCl_4·xH_2O$, Pt 48%) under magnetic stirring. Then, 0.6 mL of a 2.0 wt.% aqueous solution of polyvinyl alcohol (PVA, 80%) was added to the solution, and the system was stirred for an additional time of 5 min. A freshly prepared sodium borohydride aqueous solution (14.0 mg diluted in 5 mL water) was added dropwise to the solution under stirring, which caused a changing color of the solution instantly. Before adding the support, the pH of the solution was adjusted to 3, by using a 5% aqueous solution of HCl. Then, 250 mg of the support was added to the sol previously prepared and stirred for 2 h. The suspension produced was centrifuged at 2500 rpm for 5 min, washed 2 times with deionized water and once with ethanol, and the catalyst was dried in an oven at 70 °C for 12 h before storage in an amber bottle and placed in the desiccator. Monometallic counterparts, i.e., $Au/SrCO_3$ and $Pt/SrCO_3$, were prepared with a similar procedure; the amount of NPs was considered to provide 2.0 wt.% of metal on the support.

Catalyst reactions

The oxidation reactions were performed in a 100 mL Fischer-Porter glass reactor at 100 ℃ and 3 bar of O_2, except when mentioned in the optimization procedures. In a typical reaction, 43.5 mg of the catalyst, 33.5 mg of K_2CO_3, and 0.5 mL of benzyl alcohol were added into the reactor. The reaction was performed for 2.5 h under magnetic stirring. To analyze the performance of the catalysts in this reaction, 10 µL of the final solution were collected and added to 1 mL of CH_2Cl_2 and analyzed by gas chromatography (GC). The injection in the equipment was performed by using 1 µL of the previously prepared solution. The products were analyzed by using a Shimadzu QP2010 GC equipment, with an rtx-wax capillary column and a flame ionization detector (FID). The GC mass balance was based on the substrate charged using *p*-xylene as an internal standard, and the peaks for product detection were based on the retention times of commercial standards. The retention times were: 5.2, 7.4, 10.4, and 12.1 min for benzaldehyde, benzyl alcohol, benzyl benzoate, and benzoic acid, respectively. The conversion, selectivity, and yield were calculated using the areas of the GC peaks, which were corrected using response factors obtained by calibration curves. Specifically:

Conversion:

$$C(\%) = \frac{MS}{MS_0} \times 100 \qquad (1)$$

where C(%) is the conversion, MS is the total moles of the substrate reacted and MS_0 is the initial moles of the substrate.

Selectivity:

$$S(\%) = \frac{MPI}{MAP} \times 100 \qquad (2)$$

where S(%) is the selectivity, MPI is the moles of the product of interest and MAP is the moles of all the products.

Yield:

$$Y(\%) = C \times S \qquad (3)$$

where Y(%) is the yield, C is the conversion and S is the selectivity.

Catalyst characterization

The $Au_xPt_y/SrCO_3$ catalyst selected by the experimental data was characterized by STEM. The images of the as-prepared and spent (after the 5th run) materials were obtained with an FEI Tecnai G² F20 transmission electron microscope (Thermo Fisher Scientific, Massachusetts, USA) operating at 200 kV with an energy dispersive spectrometer (EDS). Energy-dispersive X-ray spectroscopy was recorded to obtain the element distribution maps. The samples for microscopy were prepared by drop-casting an isopropanol suspension of the materials over a grid comprised of carbon-coated copper, followed by drying under ambient conditions. The X-ray diffraction pattern (XRD) of the selected catalysts was recorded on an XRD-6000 diffractometer (Shimadzu Corp, Kyoto, Japan) with Cu Kα radiation (1.5418 Å), operating at 40 kV and 40 mA. The Rietveld refinement was performed using Rex 0.8.2 software.[26] The XPS spectra were obtained with ECSA plus spectrometer system equipped with an EA 125 hemispherical analyzer and XM 1000 monochromated X-ray source (Scientia Omicron, Uppsala, Sweden) in Al K (1486.7 eV). The source of XRD was used with a power of 280 W, as the spectrometer worked in a constant pass energy mode of 50 eV. The XPS spectra calibration for the charge accumulation was performed using C 1s peak ((binding energy (BE) = 284.8 eV). The metal content (before and after the 5th run) was determined by FAAS, using an AA-6300 Atomic Absorption Spectrophotometer (Shimadzu Corp, Kyoto, Japan). The digestion procedure of the samples was performed using concentrated nitric and hydrochloric acids in the ratio of 1:3 (HNO_3:HCl) at the heating of 115 °C for 2 h. The parameters of the catalyst's surface were determined by the Brunauer-Emmett-Teller method (BET) in a relative pressure range of 0.07 < P/Po < 0.3. The average pore diameter was determined by the Barret, Joyner and Halenda method (BJH). The gas chromatography analyses were carried out in a Shimadzu 2010 Chromatograph (Shimadzu Corp, Kyoto, Japan) equipped with flame ionization detector (FID) and a Carbowax capillary column. The computational optimization was performed in density functional theory DFT/B3LYP,[27-29] combining the basis set SDD,[30] using the software Gaussian G09.[31] In these calculations, the cubic gold unit cell was described as a cluster model consisting of 14 atoms (Au_{14}). The space group Fm-3m was used and acquired from CIF file obtained in COD Crystallography Open Database website.[32-36] All the fully optimized geometries were characterized by vibrational frequency calculations, which showed only real frequencies. The HOMO-LUMO gap energy was obtained from optimized structures in vacuum conditions. All graphical representations of clusters were produced using the JP-minerals VESTA software, version 3.[37]

Results and Discussion

Catalytic assessment of mono- and bimetallic catalysts, DFT calculation, and elemental mapping

Previously, some of us have demonstrated that strontium-based catalytic supports present remarkable effects on the oxidation of benzyl alcohol under O_2 pressure, an important feature not explored in the literature. However, we have observed that SrO is not stable under air conditions, which hampered its direct application; $Sr(OH)_2$ the phase obtained in higher amount when a calcination procedure was performed at 1100 °C and the material was cooled down to room temperature.[20,21] Here, we decided to scrutinize the possibilities that other strontium phase would present. In that matter, commercial $SrCO_3$ was a straightforward choice once it was one of the phases obtained before.[20] In addition, $SrCO_3$ is cheaper than many other materials largely used as support for catalytic applications, e.g., Al_2O_3, TiO_2, and CeO_2, and presents unique electronic properties,[35] which can be beneficial to the activity and/or selectivity of catalysts.

After the support choice, it is important to wisely select the metal(s) that will act as active species. Gold NPs are highly used for alcohol oxidations once it is believed that they are crucial for the substrate hydrogen abstraction.[36] However, alloying Au NPs with other noble metals leads to an enhancement in the performance of the catalyst, a decrease in the deactivation process, and selectivity improvement.[37] For that, once the efficiency is highly pursued, the atomic ratio of the metals is essential in terms of activity and product distribution, and Pt is a good candidate for catalyst performance improvement.[38]

To analyze the necessity of a second metal for the system, monometallic catalysts were prepared, $Au/SrCO_3$ and $Pt/SrCO_3$, using the sol immobilization method with PVA as stabilizer and $NaBH_4$ as reducing agent, and the results are displayed in Table 1. All yields and selectivity of reaction have been analyzed by gas chromatography.

The support itself did not present any activity (entry 1), while the monometallic catalysts slowly converted benzyl alcohol (**1**, Scheme 1, Table 1) without base addition; the $Au/SrCO_3$ catalyst (entry 2) resulted in oxidation products without a specific selectivity - producing benzaldehyde (**2**), benzoic acid (**3**), and benzyl benzoate (**4**) - whereas $Pt/SrCO_3$ catalyst (entry 3) was observed as more selective, presenting a slightly higher chemoselectivity to the partially oxidized product. Its lower activity is expected since platinum-based catalysts undergo to the partial oxidation of the metal surface by O_2 and present poisoning by strong chelating products.[39] Such results showed that the intrinsic basicity

Table 1. Catalytic evaluation in the benzyl alcohol oxidation using monometallic catalysts[a]

entry	Catalyst	Conversion / %	Selectivity / %		
			2	**3**	**4**
1	$SrCO_3$	0	–	–	–
2	$Au/SrCO_3$	6	44	9	47
3	$Pt/SrCO_3$	1	58	–	42
4	$Au/SrCO_3$[b]	74	60	40	–
5	$Pt/SrCO_3$[b]	2.4	68	–	32

[a]Reaction conditions: **1** (4.8 mmol), substrate:catalyst ratio = 1000, P_{O_2} = 3 bar, time = 2.5 h; [b]Addition of 0.24 mmol of K_2CO_3.

the support holds is not enough for the reaction occurring at an acceptable rate, as we have observed before for the $Sr(OH)_2$. Thus, K_2CO_3 was chosen as an external base for the maintenance of the hydrogen abstraction,[36] favoring the desorption of intermediates, which would block active sites of the catalyst.[40]
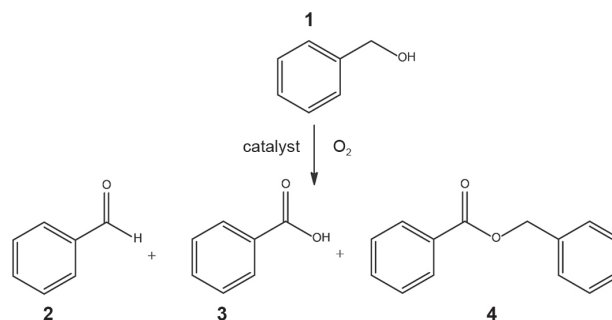
Scheme 1. Oxidation of **1** (benzyl alcohol) to form **2** (benzaldehyde), **3** (benzoic acid), and **4** (benzyl benzoate).

The $Au/SrCO_3$ catalyst (entry 4) presented a noteworthy enhancement not only in the activity (74%) but also in the selectivity for benzaldehyde (**2**) (60%). Some of us have shown that a gold catalyst supported in basic support comprised of MgO covering $MgFe_2O_4$ presented similar selectivity, but a significantly lower conversion (51%).[41] Also, commercial supports with acidic characteristics were used before - SiO_2, TiO_2, and Al_2O_3 - and any similar activity was achieved.[17] Also, Nozaki *et al.*[42] prepared some alloys using Al, Ce, and Au for the oxidation of benzyl alcohol and obtained lower conversions than the obtained here. Therefore, metal-support interactions take place in this reaction system, and the adherence of metal on the structure may explain the observed differences.[43,44] The $Pt/SrCO_3$ catalyst (entry 5) activity was not mostly affected by the presence of the base, although its selectivity presented some changing, producing more benzaldehyde (**2**).

The data obtained suggested an important role of the support, apart from the importance of the K_2CO_3 addition;

thus, we have decided to produce a bimetallic system to explore the synergy between the support, Au, and Pt. For that, Au$_x$Pt$_y$/SrCO$_3$ catalysts were prepared in different Au:Pt atomic ratios by the same procedure to obtain an efficient catalysis system. The atomic ratio was confirmed by FAAS.

The band-gap energy is the energy difference between the highest occupied orbital (HOMO) and the lowest unoccupied orbital (LUMO), which contains information about the frontier molecular orbitals in a crystalline material. Literature has been proposed that the HOMO-LUMO gap (E$_{gap}$) may be used as a descriptor of catalytic activity.[45] Thus, as an initial screening, analysis using DFT calculations with Au$_{14}$Pt and Au$_{14}$Pt$_2$ clusters allow us to have some interesting insights since direct HOMO-LUMO gap (E$_{gap}$) value estimations are obtained (Table 2).

Table 2. E$_{gap}$ calculated using DTF calculations

Energy / eV	Au$_{14}$	Au$_{14}$Pt (a)	Au$_{14}$Pt (b)	Au$_{14}$Pt$_2$ (a)	Au$_{14}$Pt$_2$ (b)
LUMO	−4.01	−4.61	−4.28	−4.75	−4.32
HOMO	−5.73	−5.45	−5.39	−5.41	−5.42
E$_{gap}$	1.72	0.84	1.11	0.66	1.10

LUMO: lowest unoccupied orbital; HOMO: highest occupied orbital; E$_{gap}$: HOMO-LUMO gap.

It is important to mention that Au$_{14}$ structure was used as a unit cell to enable the Pt atoms position changes, which made possible the assessment of the energies. The insertion process of one Pt on the Au cluster surface presents a considerable reduction on the E$_{gap}$ of the system. In addition, the position of such atom insertion matters (Figure 1). When the Pt atom is positioned as in Figure 1B, there is a reduction of 0.88 eV, while when its position is changed, the reduction of E$_{gap}$ is 0.61 eV (Figure 1C). It is expected that the same is obtained, i.e., other Pt insertion induces an E$_{gap}$ reduction. When the atoms are placed as in Figure 1D, the E$_{gap}$ does not seem to present a considerable reduction (0.62 eV), which suggests that the insertion of a new Pt atom is pointless. However, when the position is changed, a remarkable reduction is observed; 1.06 eV lower than the E$_{gap}$ of the bare gold cluster. Thus, the insertion of Pt atoms may be interesting to the reduction of the energy of the system, directly affecting its catalytic performance. Synthesis method does not allow us to have such control of atoms position, and the support effects need to be considered, we decided to test the best Au:Pt atomic ratio experimentally.

Thus, we aimed to associate both metals in an attempt to obtain a better performance in terms of activity and selectivity. Figure 2 presents the catalytic activity in the solvent-free oxidation of benzyl alcohol using the
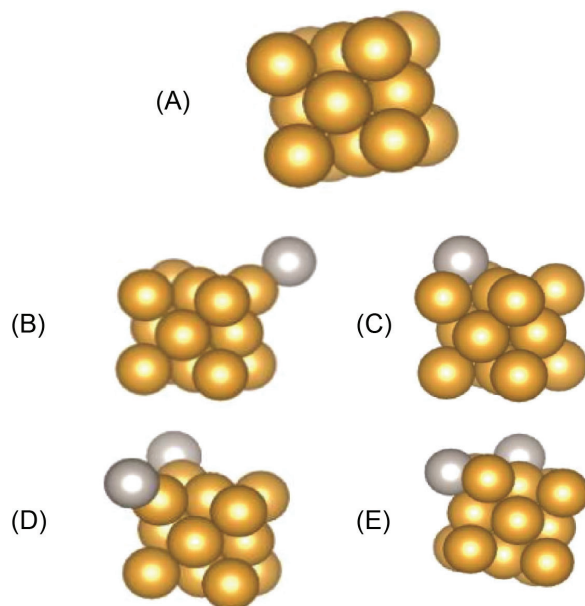

Figure 1. Predicted structure of the interaction between gold and platinum atoms. (A) Au$_{14}$; (B) Au$_{14}$Pt (a); (C) Au$_{14}$Pt (b); (D) Au$_{14}$Pt$_2$ (a); (E) Au$_{14}$Pt$_2$ (b).

as-synthesized materials: Au$_{14}$Pt$_2$, Au$_{14}$Pt$_{10}$, Au$_{14}$Pt$_{14}$, Au$_{14}$Pt$_{28}$, and Au$_{14}$Pt$_{42}$, supported in SrCO$_3$ (all the metal ratios were calculated to present 2% of uptake over the support). Under not optimized reaction conditions (100 °C, 2.5 h, 3 bar of O$_2$, 0.5 mL of alcohol, 0.24 mmol of K$_2$CO$_3$), we have observed that the increasing uptake of Pt has a noteworthy effect on the selectivity, i.e., more Pt, more selective is the system for benzaldehyde (**2**). In the other hand, the diminishing on the Au loading presents a decreasing activity, which is by the previously presented results for monometallic materials, once the activity for the Au-based material was acceptable, but the selectivity for the Pt-based system presented a higher production of benzaldehyde (**2**). Thus, we believe that the activity is not related to the Au concentration reduction, but
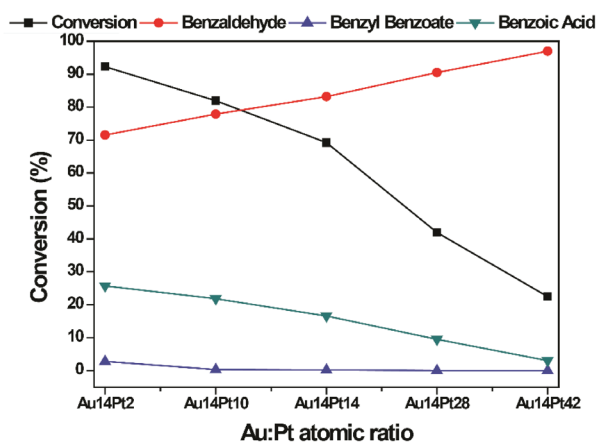

Figure 2. Influence of Au:Pt atomic ratio on the performance of Au$_x$Pt$_y$/SrCO$_3$ catalysts for oxidation of benzyl alcohol with base addition. All the results are shown in selectivity to each product of the reaction.
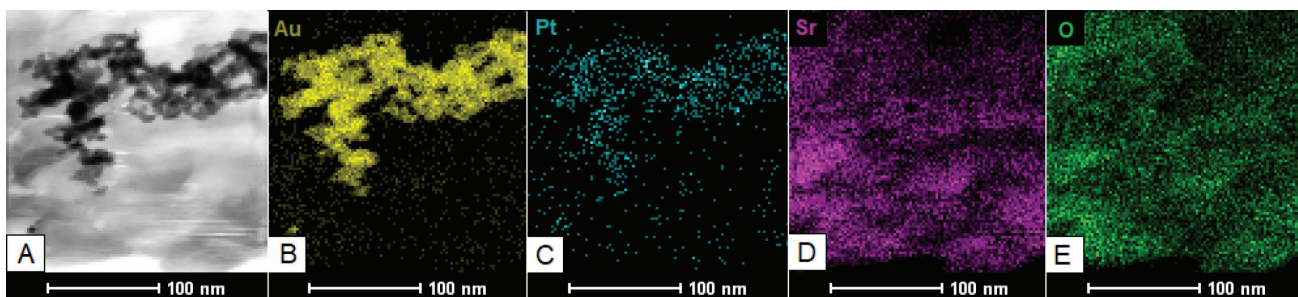
Figure 3. The morphology of the as-prepared $Au_{14}Pt_2/SrCO_3$ catalyst in the spectrum image scanning (A) and the STEM-EDS elemental map images of Au, Pt, Sr, and O (B, C, D, E, respectively).

low activity can be associated with the covering of the Au atoms, leaving less active sites available for the catalysis. The tendency that Figure 2 shows is that the activity is directly related to the Au atoms exposed to the reaction medium; nevertheless, the selectivity is associated with the synergy between Au and Pt atoms.

One can notice that the balance between selectivity and activity was obtained in the $Au_{14}Pt_2$ system since it achieved a higher yield. This result is quite interesting since Villa *et al.*,[24] using TiO_2 as support, observed the highest activity of a set of catalysts with a similar Au:Pt configuration, suggesting that gold-platinum systems are ruled more by the metal composition, however with some degree of support interactions, once the catalyst area ($4.6 m^2 g^{-1}$) and pore diameter ($233.4 Å$) of our system is not significant to explain such results.

To shed some light on the performance featured, mapping in STEM mode was analyzed since it enables direct visualization of the compositional characteristic of the catalyst comprised of Au:Pt atomic ratio of $Au_{14}Pt_2$. Figure 3A presents the catalyst in the spectrum image scanning, while Figures 3B and C illustrate the STEM-EDS images for the as-synthesized catalyst for Au and Pt. Figure 3B displays that the catalyst presents Au-rich areas, while some NPs are spread all over the support. The same is observed in the Pt mapping (Figure 3C). Apparently, the metals are always overlapped with each other, suggesting the formation of an AuPt alloy, corroborating the discussion on the gold covering by the Pt atoms. However, Wanjala *et al.*[46] claim that that nanoscale alloying of phase segregation of AuPt nanoparticles can be completely confirmed by just associating massive experimental data and theoretical studies; thus, several configurations of the metals are possible, going though alloyed, partially alloyed/partially phase-segregated, or completely phase-segregated bimetallic NPs.

Rietveld refinement, XPS, and mechanism insights

The phase composition and chemical state of the metallic species were analyzed employing XRD and XPS. Once we aimed to bring some mechanistic insights, the knowledge of the specific system under consideration is highly important. Figure 4 displays the XRD pattern of $Au_{14}Pt_2/SrCO_3$ catalyst. The diffraction pattern was indexed to only one crystalline phase: orthorhombic $SrCO_3$ (ICSD 15195). The data were refined by using the Rietveld method to ensure the information on the purity of the crystalline phase and the refined unit cell parameters for the $SrCO_3$ phase, with space group Pmcn, were found to be a = 5.09 Å, b = 8.37 Å and c = 6.02 Å.
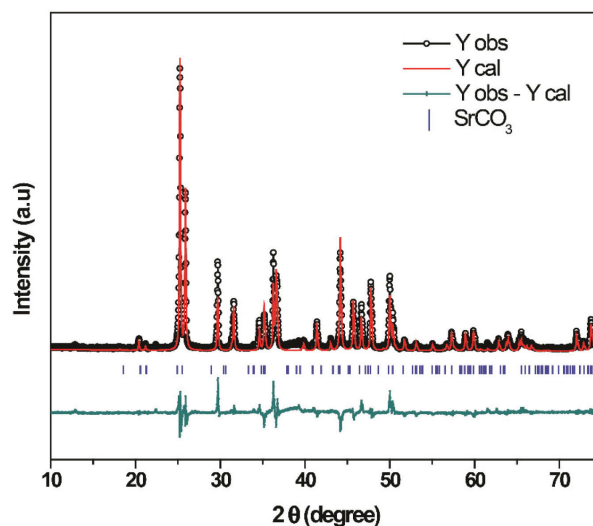

Figure 4. X-ray diffraction patterns $Au_{14}Pt_2/SrCO_3$ catalyst.

The low concentration of metal NPs hindered their observation by using XRD; thus, XPS measurements were performed. The survey scan of the material (Figure 5A) revealed the presence of Au, Pt, Sr, O, and C, as expected. However, Cl was also observed, which is from vestiges of the metals salt precursors. Figures 5B-5C show the deconvolution of the high-resolution Au 4f, with binding energies suggesting Au^0 species (Au $4f_{7/2}$ = 83.5 eV; Au $4f_{5/2}$ = 87.2 eV), and Pt 4f binding energies suggesting Pt^{2+} (Pt $4f_{5/2}$ = 74.2 eV) and Pt^0 (Pt $4f_{7/2}$ = 70.94). Electronic interactions between the Pt and Au within the particles are responsible for the values herein presented. Moreover, the

catalyst showed the existence of Pt^{2+} species because the surfaces of Pt particles might have been oxidized during the preparation process. The lower intensity of the Pt 4f peak as compared to the Au 4f peak is in accordance with the lower concentration of Pt on the catalyst support.

Based on the experimental data presented, we can comment on the reaction mechanism for benzaldehyde production once it seemed that the increasing amount of Pt atoms directly affect the production of this partially oxidized product (Figure 6). The mechanism illustrates that the reaction proceeds with the synergy between the Au and Pt NPs. In the first step (I), benzyl alcohol interacts with Au atoms, while the base (B$^-$) promotes the abstraction of the proton from the substrate. Then, an alkoxide intermediate (II) is formed, which goes through coordination with Pt atoms to form an unstable metal–H

bond (metal-alcoholate). The intermediate suffers β-hydride elimination, releasing benzaldehyde, and forming metal-hydride species (III). Molecular oxygen is activated in the electron-rich surface of the metals and removes the H from the alloy surface, restoring the catalyst.

Influence of the reaction conditions on the oxidation reaction

After the choice of catalyst composition (Au$_{14}$Pt$_2$/SrCO$_3$) and the association of the physical-chemical parameters with the experimental data obtained, optimization conditions were pursued in order to improve the catalytic performance of the catalyst; specifically, the temperature and pressure. We have decided not to change the base addition, once it would lead to a higher selectivity to benzoic acid, which was not the desired product.
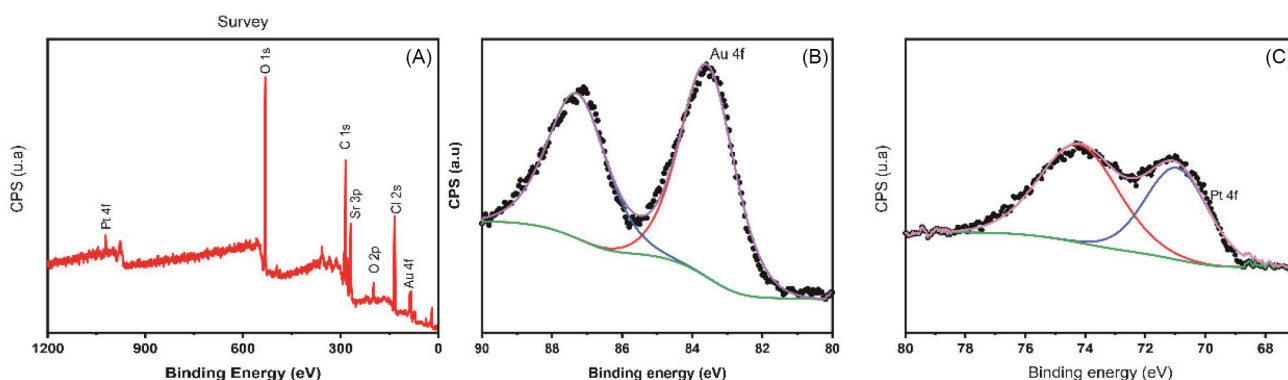

Figure 5. XPS analysis. (A) Survey; (B) Au 4f; (C) Pt 4f.
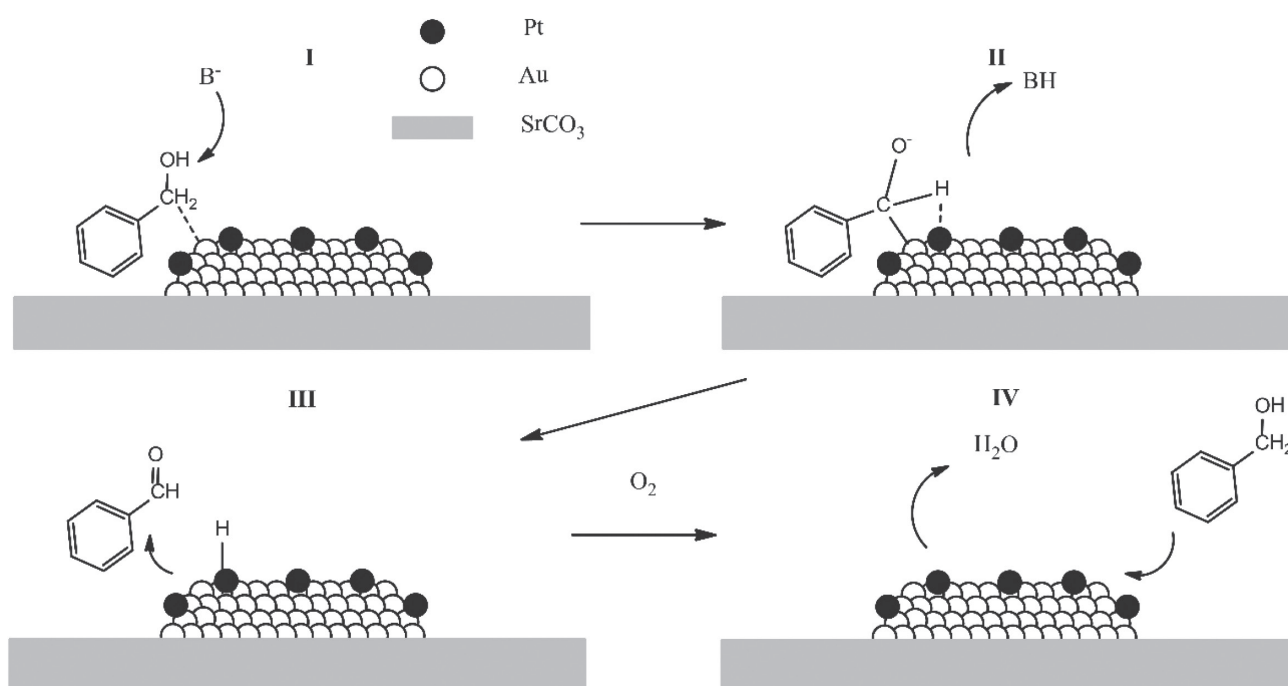

Figure 6. Possible mechanism pathway for the formation of benzaldehyde.

A temperature screening was performed from 80 to 120 °C (Table 3). One can notice that the catalyst presented a significant conversion even at 80 °C (entry 6), albeit with low selectivity for benzaldehyde. From 90 to 100 °C (entries 7 and 8), an increase in the conversion and selectivity were obtained. Using 110 °C as the system temperature (entry 9), the selectivity to the partially oxidized product was directly affected, producing more benzoic acid that at 100 °C. At 120 °C, the selectivity to benzoic acid was maintained; however, part of the benzaldehyde was converted to benzyl benzoate. Thus, it is clear that the selectivity of the system is adversely affected by the temperature increase. The best condition regarding temperature was 100 °C.

Table 3. Catalytic evaluation in the benzyl alcohol oxidation using the $Au_{14}Pt_2/SrCO_3$ catalyst with different temperatures

entry	Temperature / °C	Conversion / %	Selectivity / %		
			2	3	4
6	80	47	61	36	3
7	90	71	63	35	2
8	100	92	72	26	2
9	110	94	62	36	2
10	120	98	50	37	13

Reaction conditions: **1** (4.8 mmol), substrate:catalyst ratio = 1000, P_{O_2} = 3 bar, time = 2.5 h.

Interesting, the pressure also presents an effect on the performance of the catalyst (Table 4), which is in accordance with the proposed mechanism. As stated, the O_2 is important to the catalyst restoring, after the benzaldehyde formation. However, we are driven to believe that an increase in the pressure promotes the full oxidation of the substrate, which is expected. Thus, 1 bar (entry 11) is the best condition for benzaldehyde formation. Any pressure augmentation (entries 12-14) causes a diminishing on the selectivity to benzaldehyde, producing more benzoic acid. This tendency was clear, being the reason why higher pressures were not tested. Considering the overall performance of the catalyst, the yield is higher with P_{O_2} = 3 bar, which was the pressure used in the recycling experiments.

Recycling tests

After the previous experiments, we realized the best conditions were 100 °C, 3 bar of O_2, and 0.24 mmol of K_2CO_3. Therefore, recycling tests were performed (Figure 7). The $Au_{14}Pt_2/SrCO_3$ was able to maintain its performance (activity and selectivity) up to 5 runs, without metal leaching (confirmed by FAAS), i.e., the uptake of 2.0 wt.% was maintained.

Table 4. Catalytic evaluation in the benzyl alcohol oxidation using the $Au_{14}Pt_2/SrCO_3$ catalyst with different pressure

entry	Pressure / bar	Conversion / %	Selectivity / %		
			2	3	4
11	1	80	79	20	1
12	2	86	77	23	–
13	3	92	72	26	2
14	4	94	67	33	–

Reaction conditions: **1** (4.8 mmol), substrate:catalyst ratio = 1000, temperature = 100 °C, time = 2.5 h.
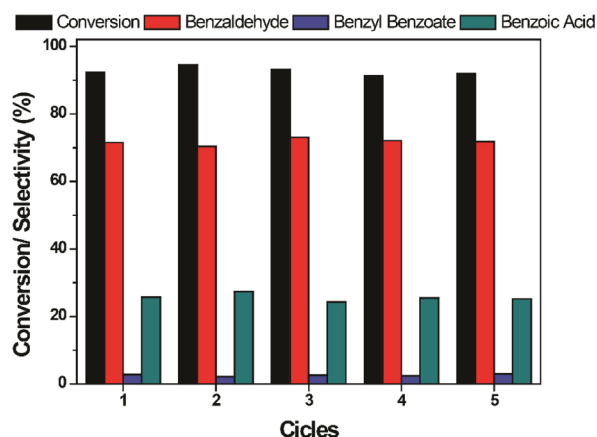

Figure 7. Recycling tests for the $Au_{14}Pt_2/SrCO_3$ catalyst in benzyl alcohol under optimized reaction conditions.

Also, the STEM-EDS images for the catalyst after the 5th run showed great similarity to the distribution of Au and Pt presented for the as-synthesized catalyst, suggesting the possibility of more runs (Figure 8).

Conclusions

Au-Pt NPs stabilized with PVA in an aqueous solution were impregnated on strontium carbonate for the solvent-free oxidation of benzyl alcohol. The application of strontium-based materials as support for the oxidation of alcohols is not properly explored in the literature; thus, our group has been working on that. We have proposed that the support presents an important role in the activity of the catalyst due to metal-support interactions; however, the Au-Pt composition was crucial for the selectivity of the system. More Pt is added in the final composition of the catalyst, more selective is the catalyst, although the activity is compromised. Bearing this in mind and based on a bunch of experimental data that includes catalytic assays and physical-chemical analyses that allowed us to specifically know the material characteristics, we have brought some insights on the mechanism of the bimetallic catalyst.
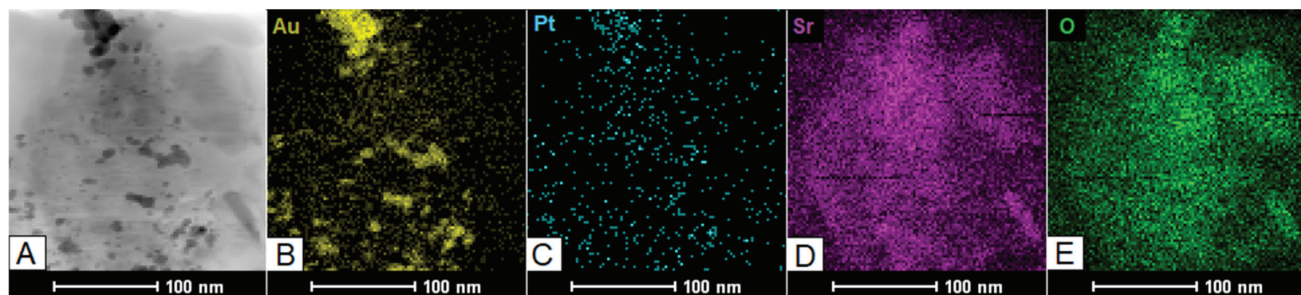
Figure 8. The morphology of the Au$_{14}$Pt$_2$/SrCO$_3$ catalyst after the 5th run in the spectrum image scanning (A) and the STEM-EDS elemental map images of Au, Pt, Sr, and O (B, C, D, E, respectively).

Considering the yield of the system, the Au$_{14}$Pt$_2$/SrCO$_3$ seemed to be the best composition choice. After ensuring the system was being used in its best conditions, we performed recycling experiments that showed the catalyst maintained its performance up to 5 runs without changing its physical characteristics, with no leaching, and with the possibility of more runs.

Acknowledgments

References

1. Zhu, X.; Guo, Q.; Sun, Y.; Chen, S.; Wang, J.; Tang, Y.; Duan, X.; Chen, D.; Wan, Y.; Wu, M.; Fu, W.; *Nat. Commun.* **2019**, *10*, 1428.

2. Mankad, N. P.; *Chem. - Eur. J.* **2016**, *22*, 5822.

3. An, K.; Somorjai, G. A.; *Catal. Lett.* **2015**, *145*, 233.

4. Kimura, H.; *Appl. Catal., A* **1993**, *105*, 147.

5. Garcia, R.; Besson, M.; Gallezot, P.; *Appl. Catal., A* **1995**, *127*, 165.

6. Mallat, T.; Baikeic, A.; *Catal. Today* **1994**, *19*, 247.

7. Prati, L.; Rossi, M.; *J. Catal.* **1998**, *176*, 552.

8. Prati, L.; Martra, G.; *Gold Bull.* **1999**, *32*, 96.

9. Porta, F.; Prati, L.; Rossi, M.; Coluccia, S.; Martra, G.; *Catal. Today* **2000**, *61*, 165.

10. Zhang, L.; Gong, J.; *Chem. Soc. Rev.* **2016**, *45*, 3916.

11. Ma, M.; Hansen, H. A.; Valenti, M.; Wang, Z.; Cao, A.; Dong, M.; Smith, W. A.; *Nano Energy* **2017**, *42*, 51.

12. Silva, T. A. G.; Teixeira-Neto, E.; López, N.; Rossi, L. M.; *Sci. Rep.* **2014**, *4*, 5766.

13. Villa, A.; Wang, D.; Sucd, D. S.; Prati, L.; *Catal. Sci. Technol.* **2015**, *55*, 55.

14. Chen, T.; Rodionov, V. O.; *ACS Catal.* **2016**, *6*, 4025.

15. Jiang, B.; Tang, Z.; Liao, F.; Lin, H.; Lu, S.; Lia, Y.; Shao, M.; *J. Mater. Chem. A* **2017**, *5*, 21903.

16. Tan, C.; Sun, Y.; Zheng, J.; Wang, D.; Li, Z.; Zeng, H.; Jing, L.; Jiang, L.; *Sci. Rep.* **2017**, *7*, 6347.

17. Gualteros, J. A. D.; Garcia, M. A. S.; Silva, A. G. M.; Rodrigues, T. S.; Cândido, E. G.; Silva, F. A.; Fonseca, F. C.; Quiroz, J.; Oliveira, D. C.; Torresi, S. I. C.; Moura, C. V. R.; Camargo, P. H. C.; Moura, E. M.; *J. Mater. Sci.* **2019**, *54*, 238.

18. Brett, G. L.; He, Q.; Hammond, C.; Miedziak, P. J.; Dimitratos, N.; Sankar, M.; Herzing, A. A.; Conte, M.; Lopez-sanchez, J. A.; Kiely, C. J.; Knight, D. W.; Taylor, S. H.; Hutchings, G. J.; *Angew. Chem.* **2011**, *50*, 10136.

19. Corma, A.; Iborra, S.; *Adv. Catal.* **2006**, *49*, 239.

20. Castro, K. P. R.; Garcia, M. A. S.; Abreu, W. C.; Sousa, S. A. A.; Moura, C. V. R.; Costa, J. C. S.; Moura, E. M.; *Catalysts* **2018**, *8*, 83.

21. Pereira, L. N. S.; Ribeiro, C. E. S.; Tofanello, A.; Costa, J. C. S.; de Moura, C. V. R.; Garcia, M. A. S.; de Moura, E. M.; *J. Braz. Chem. Soc.* **2019**, *30*, 1317.

22. Yang, G.; Shao, S.; Ke, Y.; Liu, C.; Ren, H.; Dong, W.; *RSC Adv.* **2015**, *5*, 37112.

23. Sánchez, B. S.; Gross, M. S.; Querini, C. A.; *Catal. Today* **2017**, *296*, 35.

24. Villa, A.; Jouve, A.; Trujillo, F. J. S.; Motta, D.; Prati, L.; Dimitratos, N.; *Catalysts* **2018**, *8*, 54.

25. Miedziak, P. J.; He, Q.; Edwards, J. K.; Taylor, S. H.; Knight, D. W.; Tarbit, B.; Kiely, C. J.; Hutchings, G. J.; *Catal. Today* **2011**, *163*, 47.

26. Bortolotti, M.; Lutterotti, L.; Lonardelli, I.; *J. Appl. Crystallogr.* **2009**, *42*, 538.

27. Kohn, W.; Sham, L. J.; *Phys. Rev.* **1965**, *140*, A1133.

28. Lee, C.; Yang, W.; Parr, R. G.; *Phys. Rev. B* **1988**, *37*, 785.

29. Becke, A. D.; *J. Chem. Phys.* **1993**, *96*, 2155.

30. Schwerdtfeger, P.; Dolg, M.; Schwarz, W. H. E.; Bowmaker, G. A.; Boyd, P. D. W.; *J. Chem. Phys.* **1989**, *91*, 1762.

31. Frisch, M. J.; Trucks, G. W.; Schlegel, H. B.; Scuseria, G. E.; Robb, M. A.; Cheeseman, J. R.; Montgomery Jr., J. A.; Vreven,

T.; Kudin, K. N.; Burant, J. C.; Millam, J. M.; Iyengar, S. S.; Tomasi, J.; Barone, V.; Mennucci, B.; Cossi, M.; Scalmani, G.; Rega, N.; Petersson, G. A.; Nakatsuji, H.; Hada, M.; Ehara, M.; Toyota, K.; Fukuda, R.; Hasegawa, J.; Ishida, M.; Nakajima, T.; Honda, Y.; Kitao, O.; Nakai, H.; Klene, M.; Li, X.; Knox, J. E.; Hratchian, H. P.; Cross, J. B.; Bakken, V.; Adamo, C.; Jaramillo, J.; Gomperts, R.; Stratmann, R. E.; Yazyev, O.; Austin, A. J.; Cammi, R.; Pomelli, C.; Chterski, J. W.; Ayala, P. Y.; Morokuma, K.; Voth, G. A.; Salvador, P.; Dannenberg, J. J.; Zakrzewski, V. G.; Dapprich, S.; Daniels, A. D.; Strain, M. C.; Farkas, O.; Malick, D. K.; Rabuck, A. D.; Raghavachari, K.; Foresman, J. B.; Ortiz, J. V.; Cui, Q.; Baboul, A. G.; Clifford, S.; Cioslowski, J.; Stefanov, B. B.; Liu, G.; Liashenko, A.; Piskorz, P.; Komaromi, I.; Martin, R. L.; Fox, D. J.; Keith, T.; Al-Laham, M. A.; Peng, C. Y.; Nanayakkara, A.; Challacombe, M.; Gill, P. M. W.; Johnson, B.; Chen, W.; Wong, M. W.; Gonzalez, C.; Pople, J. A.; *Gaussian 09, Revision D. 02*; Gaussian, Inc., Wallingford, USA, 2009.

32. Merkys, A.; Vaitkus, A.; Butkus, J.; Okulic-Kazarinas, M.; Kairys, V.; Grazulis, S.; *J. Appl. Crystallogr.* **2016**, *49*, 292.

33. Gražulis, S.; Merkys, A.; Vaitkus, A.; Okuličc-Kazarinas, M.; *J. Appl. Crystallogr.* **2014**, *48*, 85.

34. Merkys, A.; Chateigner, D.; Das, A.; Serebryanaya, N. R.; Moeck, P.; Lutterotti, L.; Quiro, M.; Downs, R. T.; Bail, A. L.; *Nucleic Acids Res.* **2012**, *40*, 420.

35. Gražulis, S.; Chateigner, D.; Downs, R. T.; Yokochi, A. F. T.; Quirós, M.; Lutterotti, L.; Manakova, E.; Butkus, J.; Moeck, P.; Bailh, A. L.; *J. Appl. Crystallogr.* **2009**, *42*, 726.

36. Downs, R. T.; Hall-Wallace, M.; *Am. Mineral.* **2003**, *88*, 247.

37. Momma, K.; Izumi, F.; *J. Appl. Crystallogr.* **2011**, *44*, 1272.

38. Hu, Z.; Li, Y.; Zhang, C.; Ao, B.; *J. Phys. Chem. Solids* **2016**, *98*, 65.

39. Carrettin, S.; McMorn, P.; Johnston, P.; Griffin, K.; Kiely, C. J.; Hutchings, G. J.; *Phys. Chem. Chem. Phys.* **2003**, *5*, 1329.

40. Stratakis, M.; Garcia, H.; *Chem. Rev.* **2012**, *112*, 4469.

41. Joshi, K.; Krishnamurty, S.; *New J. Chem.* **2016**, *40*, 1336.

42. Nozaki, A.; Yasuoka, T.; Kuwahara, Y.; Ohmichi, T.; Mori, K.; Nagase, T.; Yasuda, H. Y.; Yamahita, H.; *Ind. Eng. Chem. Res.* **2018**, *16*, 5599.

43. Ahmadi, M.; Timoshenko, J.; Behafarid, F.; Roldan Cuenya, B.; *J. Phys. Chem. C* **2019**, *123*, 10666.

44. Shaikhutdinov, S.; *Catal. Lett.* **2018**, *148*, 2627.

45. Abbaz, T.; Bendjeddou, A.; Villemin, D.; *Arch. Curr. Res. Int.* **2018**, *14*, 1.

46. Wanjala, B. N.; Luo, J.; Loukrakpam, R.; Fang, B.; Mott, D.; Nioki, P. N.; Engelhard, M.; Naslund, H. R.; Wu, J. K.; Wang, L.; Malis, O.; Zhong, C. J.; *Chem. Mater.* **2010**, *14*, 4282.